Solar Energy 150 (2017) 13–19

Contents lists available at ScienceDirect

Solar Energy

journal homepage: www.elsevier.com/locate/solener

Rapid fabrication and photovoltaic performance of Pt-free carbon nanotube counter electrodes of dye-sensitized solar cells

Xiuting Luo [a,1], Ji Young Ahn [b,1], Young Su Park [c], Jong Man Kim [a,b,d], Hyung Woo Lee [a,b,d], Soo Hyung Kim [a,b,d,*]

[a] Department of Nano Fusion Technology, Pusan National University, 30 Jangjeon-dong, Geumjung-gu, Busan 609-735, Republic of Korea
[b] Research Institute of Energy Convergence Technology, Pusan National University, 30 Jangjeon-dong, Geumjung-gu, Busan 609-735, Republic of Korea
[c] Department of Chemical and Biological Engineering, Friedrich-Alexander-University Campus Busan, 1276 Jisa-Dong, Gangseo-Gu, Busan 618-230, Republic of Korea
[d] Department of Nano Energy Engineering, Pusan National University, 30 Jangjeon-dong, Geumjung-gu, Busan 609-735, Republic of Korea

ARTICLE INFO

Article history:
Received 20 October 2016
Received in revised form 1 April 2017
Accepted 11 April 2017

Keywords:
Dye-sensitized solar cell
Spin-coating process
MWCNT thin film
Counter electrode
Charge transfer resistance

ABSTRACT

We fabricated uniform multiwalled carbon nanotube (MWCNT) thin films on fluorine-doped tin oxide (FTO) glass substrates with controlled thickness by an easy and versatile spin-coating process (SCP). Aqueous dispersions of MWCNTs were dropped on the FTO glass substrates and spin-coated to form uniform MWCNT thin films, which were then used as the catalytic medium on the counter electrodes (CEs) of dye-sensitized solar cells (DSCs). For the DSC with an optimized MWCNT-thin-film thickness coated on the CE, the short circuit current density (J_{sc}) was more than that of the conventional Pt-based DSC (10.97 ± 0.13 mA cm^{-2} vs 9.58 ± 0.17 mA cm^{-2}), while its power conversion efficiency (*PCE*) was comparable to that of conventional DSC ($\sim$4.41 ± 0.14% and $\sim$4.69 ± 0.22%, respectively). This suggests that the accumulation of MWCNTs on the CE increases the interfacial contact area between the MWCNTs and liquid electrolyte in the DSC, allowing the rapid reduction of I_3^-. Simultaneously, it decreases the charge transfer resistance owing to rapid electron transport through the MWCNT medium with its relatively high electrical conductivity. Thus, the precisely controlled rapid accumulation of MWCNT thin films by the SCP on the CEs of DSCs is a very promising approach for replacing the expensive Pt metal that is currently used in DSC applications.

1. Introduction

Dye-sensitized solar cells (DSCs) have attracted considerable attention as next-generation solar cells due to their simple manufacturing processes and relatively low production costs (O'Regan and Gratzel, 1991). Typical DSCs consist of a TiO_2 nanoparticle accumulation layer with a sensitizing dye as the photoelectrode, a redox couple containing iodide/triiodide (I^-/I_3^-) in the electrolyte, and a Pt-coated fluorine-doped tin oxide (FTO) glass substrate as the counter electrode (CE). The polychromatic photoabsorption by the dye, fast electron transfer at the TiO_2 photoanode layer, good ion diffusivity in the electrolyte, and efficient reduction of the redox couple at the CE are the key factors that collectively determine the power conversion efficiency (*PCE*) of a DSC. When the dye is excited by sunlight, the CE transfers electrons from the external circuit to the redox couple.

Generally, Pt is used in the CEs of DSCs since it has excellent catalytic activity for the effective reduction of I^-/I_3^- and good electrical conductivity (Hauch and Georg, 2001; Gratzel, 2004; Nazeeruddin et al., 2005; Ahn et al., 2013; Halme et al., 2006; Murakami and Grätzel, 2008; Papageorgiou, 2004; Lee et al., 2010). However, it has the disadvantages of being relatively expensive and easily corroded by the liquid iodide electrolyte (Chiba et al., 2006; Olsen et al., 2000; Luo et al., 2009). These drawbacks have led to the search for proper alternatives to replace Pt catalytic films.

Various carbon nanomaterials, including singlewalled carbon nanotubes (SWCNTs), multiwalled carbon nanotubes (MWCNTs) and carbon nanoparticles (CNPs) were synthesized using aerosol/thermal CVD and spraying/compression processes, and then they were used as Pt-free CEs of DSCs. The results showed that SWCNTs, MWCNTs, and CNPs have reasonable catalytic performance (Hashmi et al., 2014; Aitola et al., 2011; Han et al., 2010; Zhang et al., 2011).

* Corresponding author at: Department of Nano Fusion Technology, Pusan National University, 30 Jangjeon-dong, Geumjung-gu, Busan 609-735, Republic of Korea.
E-mail address: sookim@pusan.ac.kr (S.H. Kim).
[1] Both X. Luo and J.Y. Ahn contributed equally to this work as the first authors.

http://dx.doi.org/10.1016/j.solener.2017.04.029
0038-092X/

MWCNTs have recently attracted strong interest as practical materials for CEs in DSCs because of their relatively low cost, large specific surface area, and good electrocatalytic activity. Furthermore, they are quite stable in general electrolytes, including the redox couple in the DSCs. Recently, polyelectrolyte-grafted MWCNTs (Han et al., 2010) and graphitic carbon nitride/MWCNT composites (Wang et al., 2016) are introduced into CEs of DSCs, which result in showing excellent electrocatalytic activity for triode reduction and low charge-transfer resistance. However, they require very complex fabrication procedures, and it is also hard to obtain uniform composites.

To use MWCNTs in the CEs of DSCs, the MWCNTs can be coated on an FTO glass substrate through various coating techniques such as electrospraying, doctor blading, electrophoretic deposition, screen printing, hydrothermal deposition, and aerosol deposition (Zhu et al., 2011; Xia et al., 2009; Benard and Chahine, 2001; Suzuki et al., 2003; Ebbesen et al., 1996; Chew et al., 2009; Chen et al., 2009; Han et al., 2010; Ko Kyaw et al., 2012; Roy-Mayhew et al., 2010; Kim et al., 2012; Cha et al., 2010; Siriroj et al., 2012; Hsieh et al., 2011; Li et al., 2010; Ahn et al., 2014; Lee et al., 2009). However, employing these techniques to coat MWCNTs on the FTO glass causes intrinsic problems in fabricating uniform MWCNT thin films; furthermore, precise control of the film thickness is challenging due to highly agglomerated and entangled characteristics of the MWCNTs in solution. Moreover, forming a nonuniform MWCNT thin film on the FTO glass substrate can eventually deteriorate electron transfer in the DSCs. Therefore, a reliable and adjustable method is required to fabricate a uniform distribution of MWCNTs on the substrate.

In this study, we employed a simple and rapid spin-coating process (SCP) to deposit a uniform MWCNT thin film on an FTO glass for use as the CE of a DSC. Furthermore, we systematically examined the photovoltaic performance of the resulting DSCs by varying the thickness of the MWCNT thin films, and then compared the results with a conventional Pt-based DSC.

2. Experimental

2.1. Preparation of MWCNT-dispersed aqueous solution

The MWCNTs (>95% purity) were purchased from CNT Co., Ltd. (Korea) and employed without further treatment. The MWCNTs, synthesized by a thermal CVD process, had an average diameter of ~20 nm and a length distribution of 1–25 μm. The specific surface area was approximately 150–250 $m^2 g^{-1}$.

To fabricate a homogeneous MWCNT-dispersed aqueous solution, we adopted the surfactant addition method. By adding an appropriate surfactant, which serves to interconnect the hydrophobic and hydrophilic surfaces, MWCNTs can be dispersed homogeneously in aqueous solution. In this experiment, carboxymethyl cellulose (CMC, Sigma Aldrich, M_w: 700,000) was used as the surfactant (Cha et al., 2010; Lee et al., 2009; Imoto et al., 2003; Takahashi et al., 2004). In CMC, the hydroxyl functional groups stabilize the MWCNT clusters and allow their homogeneous dispersion in water, probably by surrounding the MWCNT surfaces and overcoming the van der Waals attractions among the MWCNT bundles. We prepared a CMC-added MWCNT aqueous solution containing 1 wt% MWCNTs and 0.15 wt% CMC in deionized water by sonicating with a probe sonicator (Daihan Scientific Co., Ltd.) at 665 W for 30 min.

2.2. Fabrication of MWCNT-deposited CEs by SCP

MWCNT-deposited CEs were fabricated by depositing the MWCNT solution onto FTO glass substrates (SnO_2:F, 7 Ω/sq, Pilkington) by the SCP shown in Fig. 1. SCP can be divided into the following three steps the introduction of the MWCNT droplets, spinning the substrate at constant rotating speed (ω), and drying the MWCNT thin films. The first step involves dispensing sufficient MWCNT solution onto a stationary and then slowly spinning the substrate to prevent the formation of coating discontinuities caused by the drying of solution prior to reaching the substrate edge. During the spinning stage, as the FTO glass substrates are rotated at a constant speed of 3000 rpm for 20 s, the droplet is thinned by centrifugal forces until the solvent is removed, thereby increasing the viscosity to a certain degree. After forming the uniform MWCNT thin film on the FTO glass, the CE is dried on a hot plate at approximately 100 °C for 3 min to increase film adhesion to the substrate by removing the residual solvent. The thickness of the MWCNT thin film could be controlled by the number of spin-coating repetitions ($N_{coating}$). The MWCNT thin films deposited by SCP were additionally heated in an electric furnace at 350 °C for 20 min to remove the surfactant.

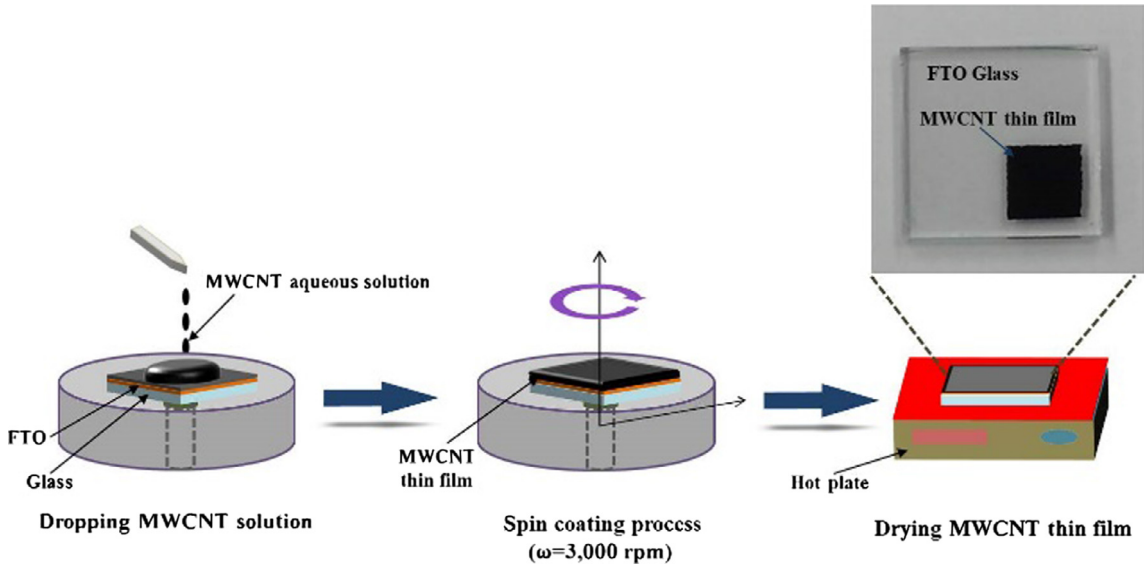

Fig. 1. Schematic of the spin-coating system for fabricating a MWCNT thin film on an FTO glass substrate.

2.3. Fabrication of DSCs

A TiO_2 nanoparticle (NP)-accumulated photocatalytic active layer was formed by a screen-printing process on an FTO glass with an active area of $0.6 \times 0.6\ cm^2$ and an average thickness of ~25 μm. To prepare the TiO_2 paste, commercially available TiO_2 NPs (P25, Degussa) were used without further treatment. The TiO_2 NPs (6 g), ethanol (15 g), acetic acid (CH_3COOH, 1 mL), and terpineol (20 g) were mixed in a vial and sonicated for 1 h. Ethyl cellulose (3 g) dissolved in ethanol (27 g) was separately prepared, and subsequently, the two solutions were mixed in a single vial for 3 min with a planetary mixer. The resulting TiO_2 NP-accumulated layer was formed on the FTO glass by the screen printing process, and then sintered in an electric furnace at 500 °C for 30 min. The sintered photocatalytic layer was immersed in anhydrous ethanol containing 0.3 mM of the Ru-dye $(Bu_4N)_2[Ru(Hdcbpy)_2\text{-}(NCS)_2]$ (N719 dye, Solaronix) for 24 h at room temperature to allow attachment of the dye molecules to the entire surface of the TiO_2 NPs. The dye-soaked TiO_2 NP-based photoelectrode was then rinsed with ethanol and dried in a convection oven at 80 °C for 10 min.

As a reference counter electrode, we also prepared a Pt-coated FTO glass substrate using ion-sputtering operated at 1.2 kV and 7 mA. The dye-adsorbed TiO_2 layer on the FTO glass and the CEs (i.e., the Pt- and MWCNT-coated FTO glasses) were assembled with a hot-melt polymer film (60 μm thickness, Surlyn®, DuPont) in a sandwich-type configuration and heated at 120 °C for 4 min. Subsequently, the iodide-based liquid electrolyte (AN-50, Solaronix) was injected into the interspace between the electrodes through a hole drilled in the CE. The hole was sealed with a cover glass using the hot-melt polymer film.

2.4. Characterization of the MWCNT thin films and photovoltaic properties of the DSCs

The morphologies of the MWCNTs and MWCNT-deposited thin films were characterized by scanning electron microscopy (SEM; PS-250, Pemtron) operated at ~20 kV.

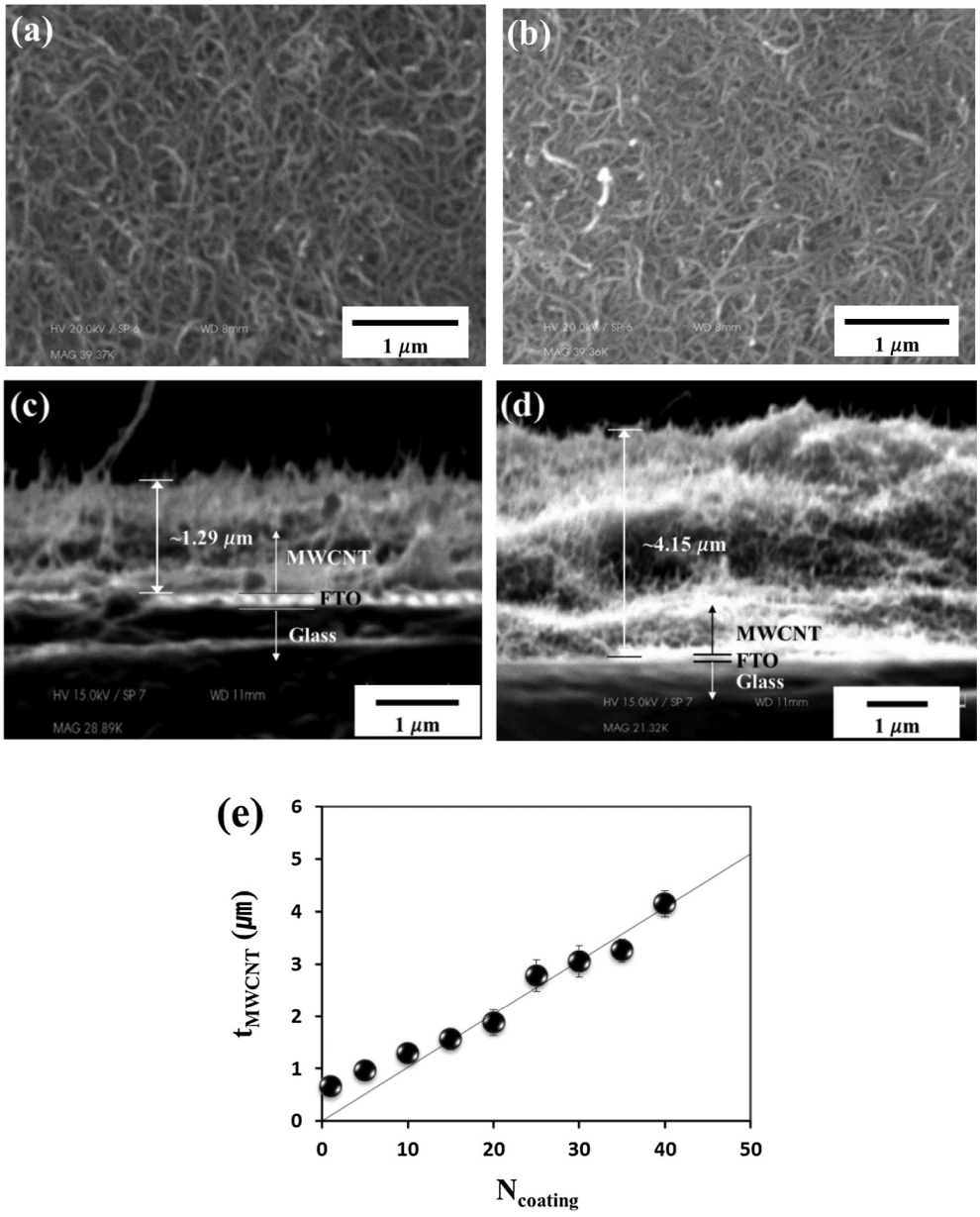

Fig. 2. SEM images (top view) of MWCNT thin films deposited with number of coating ($N_{coating}$) of (a) 10 and (b) 40, respectively. SEM images (cross sectional view) of MWCNT thin films deposited with $N_{coating}$ of (c) 10 and (d) 40, respectively. (e) The thickness of MWNCT thin films (t_{MWCNT}) as a function of $N_{coating}$.

The current density–voltage (*J–V*) characteristics of the DSCs fabricated in this study were measured under AM 1.5 simulated illumination with an intensity of 100 mW cm^{-2} (PEC-L11, Peccell Technologies Inc.). Before measurement, the intensity of sunlight illumination was calibrated using a standard Si photodiode detector with a KG-5 filter. The *J–V* curves were automatically recorded using a Keithley SMU 2400 source meter by illuminating the DSCs. The electrochemical impedance spectroscopy (EIS) measurements for the DSCs were performed under illumination at 100 mW cm^{-2}, and the explored frequency range was 0.0001–100 kHz. Here, the bias voltage and ac amplitude were set at the V_{oc} of the DSCs and 10 mV, respectively.

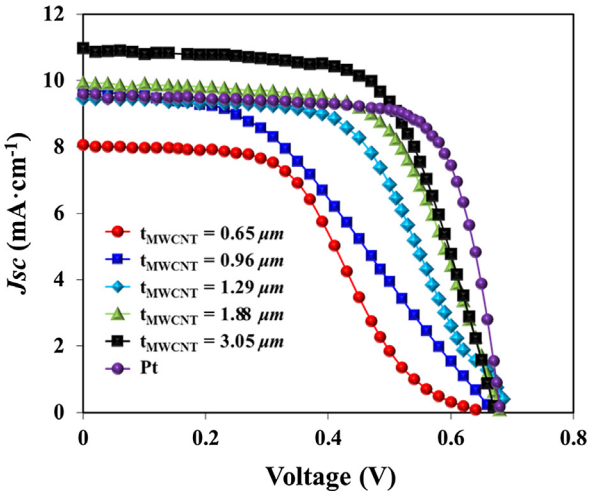

Fig. 3. Current density-voltage (*J-V*) curves for DSCs containing Pt- and various MWCNT thin films-coated counter electrodes.

3. Results and discussion

Fig. 2a and b shows the top views of the MWCNT thin films formed by SCP with 10 and 40 coating repetitions, respectively. Both spin-coated MWCNT thin films were homogeneously deposited on the FTO glass substrate. The thickness of a typical MWCNT thin film formed on the FTO glass substrate increases linearly from ~1.29 μm for 10 coats to ~4.15 μm for 40 coats, as shown in Fig. 2c and d, respectively. The average thickness of the MWCNT thin films increases linearly with increasing SCP coating number; the rate of the thickness growth was calculated as ~0.089 ± 0.01 μm per coat, as shown in Fig. 2e. The growth rate of the MWCNT thin film was determined to be 11.35 ± 0.91 μm h^{-1}, which is nearly 15 times faster than that of the aerosol deposition process (0.75 ± 0.15 μm h^{-1}) (Ko Kyaw et al., 2012). These results suggest that the thickness of a stable and uniform MWCNT thin film on the FTO glass can be precisely controlled and rapidly grown by SCP.

The effects of various MWCNT thin film thicknesses on the photovoltaic performance of DSCs were systematically examined by measuring the current density–voltage (*J–V*) characteristics under 1 sun illumination (100 mW cm^{-2}, AM 1.5G), as shown in Fig. 3. The J_{sc} and fill factor (*FF*) were enhanced with the increasing thickness of the MWCNT thin film, although V_{oc} did not show any appreciable change.

The specific photovoltaic performance of the MWCNT-based DSCs compared to the reference Pt-based DSC is shown in Fig. 4.

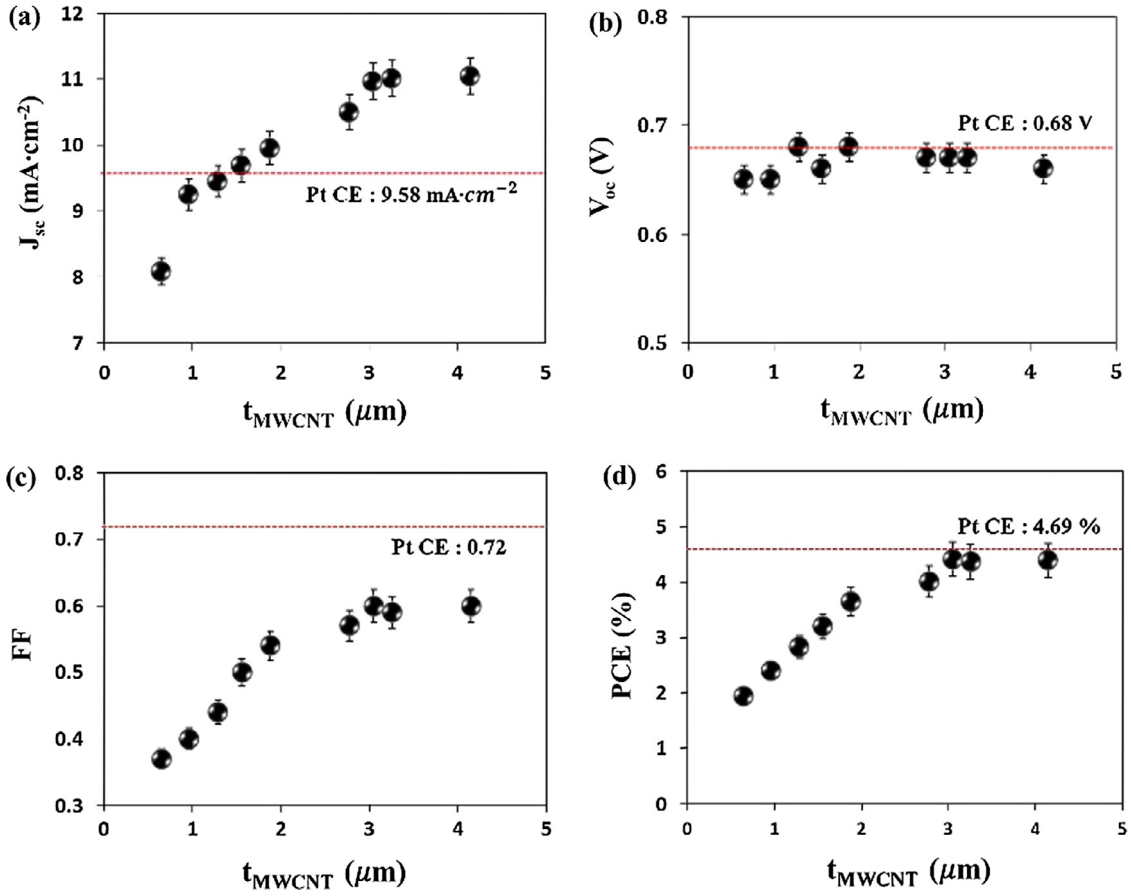

Fig. 4. Changes in photovoltaic performance ((a) J_{sc}, (b) V_{oc}, (c) *FF*, and (d) *PCE*) of DSCs by varying the thickness of MWCNT thin films.

Table 1
Summary of photovoltaic properties of various DSCs with Pt- and MWCNT-thin-film-coated counter electrodes.[a]

CE	$N_{coating}$	t_{MWCNT} (μ m)	V_{oc} (V)	J_{sc} (mA cm^{-2})	*FF*	*PCE* (%)	τ_e (ms)	R_{sh} (Ω)	R_{ct} (Ω)	R_{rec} (Ω)
MWCNT	1	0.65	0.65 ± 0.01	8.09 ± 0.09	0.37 ± 0.02	1.95 ± 0.13	1.26	5.12	1.71	66.88
	5	0.96	0.65 ± 0.01	9.25 ± 0.15	0.40 ± 0.01	2.40 ± 0.14	2.52	5.42	1.47	56.85
	10	1.29	0.68 ± 0.01	9.45 ± 0.30	0.44 ± 0.01	2.83 ± 0.20	3.06	5.09	1.38	43.64
	15	1.56	0.60 ± 0.01	9.69 ± 0.16	0.50 ± 0.01	3.20 ± 0.17	4.00	5.38	1.29	40.77
	20	1.88	0.68 ± 0.01	9.95 ± 0.12	0.54 ± 0.02	3.65 ± 0.25	5.03	5.10	1.20	36.54
	25	2.78	0.67 ± 0.01	10.50 ± 0.20	0.57 ± 0.01	4.01 ± 0.21	5.40	5.24	1.09	32.88
	30	3.05	0.67 ± 0.01	10.97 ± 0.13	0.60 ± 0.01	4.41 ± 0.14	5.50	5.18	0.95	25.43
	35	3.26	0.67 ± 0.01	11.01 ± 0.22	0.59 ± 0.01	4.37 ± 0.04	6.10	5.42	0.83	25.09
	40	4.15	0.66 ± 0.01	11.05 ± 0.17	0.60 ± 0.01	4.39 ± 0.21	6.34	5.69	0.69	25.04
Pt	–	–	0.68 ± 0.01	9.58 ± 0.17	0.72 ± 0.01	4.69 ± 0.22	5.03	5.01	1.67	11.91

[a] Note: CE = counter electrode, MWCNT = multiwalled carbon nanotubes, $N_{coating}$ = number of spin coats, t_{MWCNT} = thickness of MWCNT thin film, V_{oc} = open circuit voltage, J_{sc} = short circuit current, *FF* = fill factor, *PCE* = power conversion efficiency, τ_e = electron lifetime, R_{sh} = sheet resistance, R_{ct} = charge transport resistance, R_{rec} = recombination resistance.

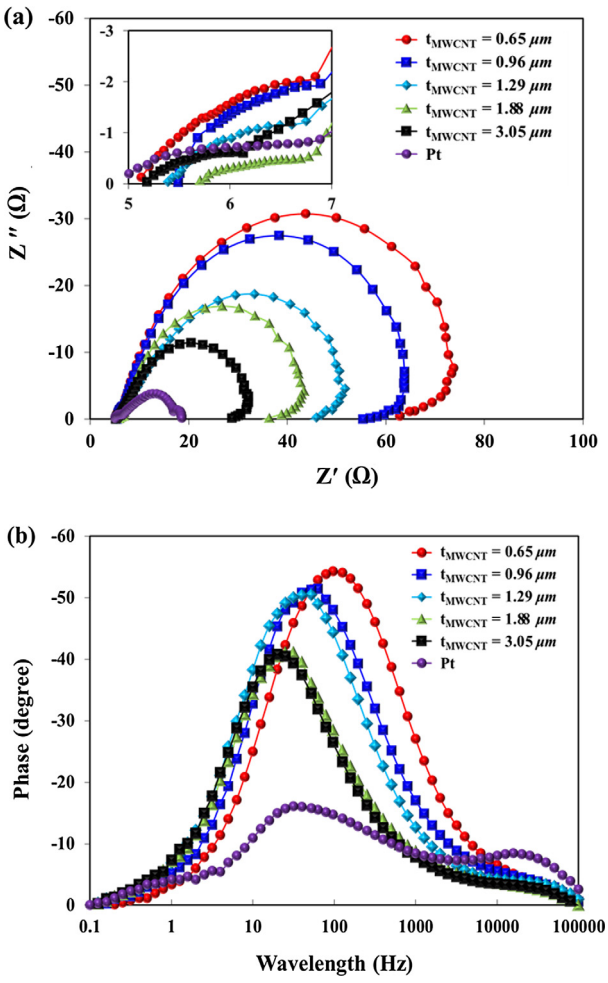

Fig. 5. (a) Nyquist plots and (b) Bode plots for DSCs containing Pt- and various MWCNT thin films-coated counter electrodes.

Here, other parameters such as the TiO_2 layer, dye, and liquid electrolyte were fixed for a direct comparison between the MWCNT- and Pt-based DSCs. Both J_{sc} and *FF* increase significantly on increasing the MWCNT thin film thickness (t_{MWCNT}) up to ~2 μm, and then appear to stabilize on further thickening the film up to ~4 μm, as shown in Table 1 and Fig. 4a and c. However, V_{oc} does not change significantly upon increasing the MWCNT film thickness, as shown in Fig. 4b. The *PCE* values of the DSCs with MWCNT CEs increase with the MWCNT thin film thickness, and then become saturated at the *PCE* of the DSC with the Pt CE (Fig. 4d). For DSCs prepared by the SCP proposed in this study, the maximum photovoltaic performance values were V_{oc} = ~0.67 V; J_{sc} = ~10.97 mA cm^{-2}; *FF* = ~0.60; and *PCE* = ~4.41%, obtained for the CE with a ~3 μm MWCNT thin film. For comparison, the photovoltaic properties of the DSC with the conventional Pt CE were V_{oc} = ~0.68 V; J_{sc} = ~9.58 mA cm^{-2}; *FF* = ~0.72; and *PCE* = ~4.69%. These results suggest that MWCNTs can be promising replacements for Pt, because the catalytic reaction at the CE in a DSC occurs effectively on the MWCNTs; moreover, simultaneously increasing the thickness of the MWCNT thin film on the CE enhances the photovoltaic performance of the DSC. This can be attributed to the increased interfacial contact area between the MWCNTs and liquid electrolyte due to the accumulation of the MWCNTs on the CE. This, in turn, results in faster completion of I_3^- reduction and decreases the charge transfer resistance owing to the rapid electron transport through the MWCNT medium with its relatively high electrical conductivity.

The foregoing results were corroborated by EIS, as shown in Table 1 and Fig. 5. The Nyquist plots shown in Fig. 5a clearly show that an increase in the thickness of the MWCNT thin film significantly reduces the charge transfer resistance at the electrolyte/CE interface (R_{ct}) Imoto et al., 2003. This is because the accumulation of MWCNT layers on the CE increases the interfacial contact area between the MWCNTs and liquid electrolyte. Also, the impedance, which occurs owing to competitive recombination at the TiO_2/dye/electrolyte interface (R_{rec}), also decreased with the thickening of the MWCNT film (Takahashi et al., 2004). With a thicker film, a faster electron exchange occurs at the CE/electrolyte interface that reduces the build-up of the I_3^- charge at the TiO_2/dye/electrolyte interface, which in turn reduces the rate of the recombination that occurs at the TiO_2/dye/electrolyte interface. This leads to a reduction in R_{rec}. The sheet resistance (R_{sh}) of the DSCs with MWCNT-based CEs is relatively independent of MWCNT film thickness and comparable to that of the DSC with the Pt-based CE. This is because the CEs are prepared on the same FTO glass, and R_{sh} is mostly affected by the electrical properties of the FTO glass when the deposition layers are sufficiently thin (Han et al., 2005). Fig. 5b shows Bode phase plots for analyzing the electron lifetime. The electron lifetime in DSCs is a central quantity to determine the recombination dynamics inside of cell which can be treated as a product of the chemical capacitance and recombination resistance. From Table 1, V_{oc} showed similar values with different thicknesses of MWCNT thin films, thus at a certain potential, recombination flow matched the photocurrent (Bisquert et al., 2009), in this case, the electron lifetime was mainly determined by J_{sc}. The maximum peak frequency shifted to a lower value with an increase in the thickness of MWCNT thin film on the CE, correspondingly, the electron lifetime ($\tau_e = [2\pi f_{max}]^{-1}$, where f_{max} is the maximum peak frequency) increased from 0.4 ms (t_{MWCNT} = ~0.65 μm) to 6.34 ms (t_{MWCNT} = ~4.15 μm). This result suggests that photogenerated

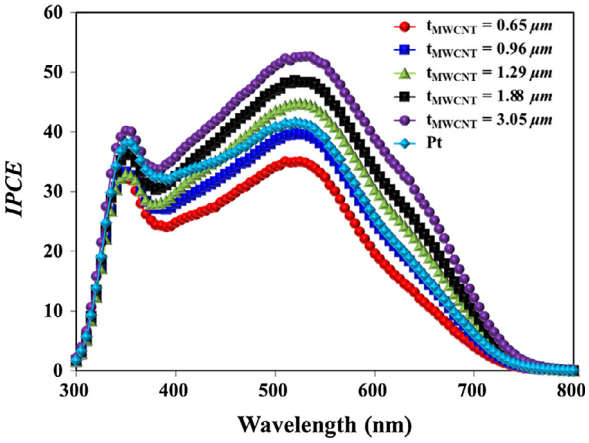

Fig. 6. The IPCE spectra of DSCs with various thicknesses of MWCNT thin films coated on counter electrodes.

electrons could further diffuse through TiO_2-coated photoelectrodes and MWCNT-coated CEs because the increase in the amount of MWCNTs on CEs significantly reduced the recombination of photogenerated electrons with dyes and electrolytes.

To understand the major factor underlying the improved PCEs of the DSCs with thicker MWCNT-thin-film-based CEs, the incident photon-to-electron conversion efficiency (*IPCE*) spectra were also measured as a function of the incident light wavelength. The *IPCE* value depends on both the absorption of light and the collection of separated charges. The *IPCE* spectra (Fig. 6) show that the DSCs with thicker MWCNT-thin-film-based CEs exhibit *IPCE* values superior to those with thinner ones under the same light intensity, suggesting that the thicker MWCNT layer functions as a more effective electron transfer medium, inherently enhancing the photovoltaic performance of the DSC, owing to the reduction of recombination between the separated electrons and the electrolyte.

4. Conclusions

Using SCP, we fabricated MWCNT thin films on CEs to examine the effects of the films on the photovoltaic performance of DSCs. By varying the number of SCP applications, the thickness of the MWCNT thin film was precisely controlled. After assembling the DSCs by depositing MWCNT thin films of various thicknesses on the CEs, their photovoltaic performance was measured and compared to that of a reference DSC with a Pt-based CE.

For the DSCs with MWCNT-thin-film-based CEs, the J_{sc}, *FF*, and *PCE* values increased significantly with the increasing thickness of the MWCNT film. The maximum *PCE* of the DSC containing the optimized film thickness (i.e., $t_{MWCNT} = \sim 3$ μm) on the CE was ~4.41%. This *PCE* value was similar to that of the conventional Pt-based DSC (4.69%), confirming that MWCNTs are highly promising as candidates to replace the expensive Pt-based CEs in DSCs. Furthermore, the SCP was proven to be a rapid and versatile method with potential for use in DSC industrial applications.

Acknowledgment

This study was supported by a 2-Year Research Grant of Pusan National University, South Korea.

References

Ahn, J.Y., Kim, J.H., Moon, K.J., Park, S.D., Kim, S.H., 2013. Synergistic effects of the aspect ratio of TiO_2 nanowires and multi-walled carbon nanotube embedment for enhancing photovoltaic performance of dye-sensitized solar cells. Nanoscale 5, 6842.

Ahn, J.Y., Kim, J.H., Kim, J.M., Lee, D.G., Kim, S.H., 2014. Multiwalled carbon nanotube thin films prepared by aerosol deposition process of use as highly efficient Pt-free counter electrodes of dye-sensitized solar cells. Sol. Energy 107, 660–667.

Aitola, K., Halme, J., Halonen, N., Kaskela, A., Toivola, M., Nasibulin, A.G., Kordás, K., Tóth, G., Kauppinen, E.I., Lund, P.D., 2011. Comparison of dye solar cell counter electrodes based on different carbon nanostructures. Thin Solid Films 22, 8125–8134.

Benard, P., Chahine, R., 2001. Determination of the Adsorption isotherms of hydrogen on activated carbons above the critical temperature of the adsorbate over wide temperature and pressure ranges. Langmuir 17, 1950–1955.

Bisquert, J., Santiago, F.F., Sero, I.M., Belmonte, G.G., Gimenez, S., 2009. Electron lifetime in dye-sensitized solar cellstheory and interpretation of measurements. J. Phys. Chem. C 113, 17278–17290.

Cha, S.I., Koo, B.K., Seo, S.H., Lee, D.Y., 2010. Pt-free transparent counter electrodes for dye-sensitized solar cells prepared from carbon nanotube micro-balls. J. Mater. Chem. 20, 659–662.

Chen, Y.S., Huang, J.H., Chuang, C.C., 2009. Glucose biosensor based on multiwalled carbon nanotubes grown directly on Si. Carbon 47, 3106–3112.

Chew, S.Y., Ng, S.H., Wang, J.Z., Novak, P., Krumeich, F., Chou, S.L., Chen, J., Liu, H.K., 2009. Flexible free-standing carbon nanotube films for model lithium-ion batteries. Carbon 47, 2976–2983.

Chiba, Y., Islam, A., Watanabe, Y., Komiya, R., Koide, N., Han, L., 2006. Dye-sensitized solar cells with conversion efficiency of 11.1%. Jpn. J. Appl. Phys. 45, L638.

Xia, Y.D., Walker, G.S., Grant, D.M., Mokaya, R., 2009. Hydrogen Storage in high surface area carbonsexperimental demonstration of the effects of nitrogen doping. J. Am. Chem. Soc. 131, 16493–16499.

Ebbesen, T.W., Lezec, H.J., Hiura, H., Bennett, J.W., Ghaemi, H.F., Thio, T., 1996. Electrical conductivity of individual carbon nanotubes. Nature 382, 54–56.

Gratzel, M., 2004. Conversion of sunlight to electric power by nanocrystalline dye-sensitized solar cells. J. Photochem. Photobiol., A 164, 3–14.

Halme, J., Toivola, M., Tolvanen, A., Lund, P., 2006. Charge transfer resistance of spray deposited and compressed counter electrodes for dye-sensitized nanoparticle solar cells on plastic substrates. Sol. Energy Mat. Sol. Cells 90, 872–886.

Han, L.Y., Koide, N., Chiba, Y., Islam, A., Komiya, R., Fuke, N., Fukui, A., Yamanaka, R., 2005. Improvement of efficiency of dye-sensitized solar cells by reduction of internal resistance. Appl. Phys. Lett. 86, 213501.

Han, J., Kim, H., Kim, D.Y., Jo, S.M., Jang, S.Y., 2010. Water-soluble polyelectrolyte-grafted multiwalled carbon nanotube thin films for efficient counter electrode of dye-sensitized solar cells. ACS Nano 4, 3503–3509.

Han, J.K., Kim, H.J., Kim, D.Y., Jo, S.M., Jang, S.Y., 2010. Water-soluble polyelectrolyte-grafted multiwalled carbon nanotube thin films for efficient counter electrode of dye-sensitized solar cells. ACS Nano 4, 3503–3509.

Hashmi, S.G., Halme, J., Ma, Y., Saukkonen, T., Lund, P., 2014. A single-walled carbon nanotube coated flexible PVC counter electrode for dye-sensitized solar cells. Adv. Mater. Interf. 1, 1300055. http://dx.doi.org/10.1002/admi.201300055.

Hauch, A., Georg, A., 2001. Diffusion in the electrolyte and charge-transfer Reaction at the platinum electrode in dye-sensitized solar cells. Electrochim. Acta 46, 3457–3466.

Hsieh, C.T., Yang, B.H., Lin, J.Y., 2011. One- and two-dimensional carbon nanomaterials as counter electrodes for dye-sensitized solar cells. Carbon 49, 3092–3097.

Imoto, K., Takahashi, K., Yamaguchi, T., Komura, T., Nakamura, J., Murata, K., 2003. High-performance carbon counter electrode for dye-sensitized solar cells. Sol. Energy Mater. Sol. Cells 79, 459–469.

Kim, H.K., Choi, H.K., Hwang, S.H., Kim, Y.J., Jeon, M.H., 2012. Fabrication and characterization of carbon-based counter electrodes prepared by electrophoretic deposition for dye-sensitized solar cells. Nanoscale Res. Lett. 7, 53.

Ko Kyaw, A.K., Tantang, H., Wu, T., Ke, L., Wei, J., Demir, H.V., Zhang, Q., Sun, X.W., 2012. Dye-sensitized solar cell with a pair of carbon-based electrodes. Appl. Phys. 45, 165103.

Lee, W.J., Ramasamy, E., Lee, D.Y., Song, J.S., 2009. Efficient dye-sensitized solar cells with catalytic multiwall carbon nanotube counter electrodes. ACS Appl. Mater. Interf. 1, 1145–1149.

Lee, Y.L., Chen, C.L., Chong, L.W., Chen, C.H., Liu, Y.F., Chi, C.F., 2010. A platinum counter electrode with high electrochemical activity and high transparency for dye-sensitized solar cells. Electrochem. Commun. 12, 1662–1665.

Li, G.R., Wang, F., Jiang, Q.W., Gao, X.P., Shen, P.W., 2010. Carbon nanotubes with titanium nitride as a low-cost counter-electrode material for dye-sensitized solar cells. Angew. Chem. Int. Ed. 49, 3653–3656.

Luo, Y., Li, D., Meng, Q., 2009. Towards optimization of materials for dye-sensitized solar cells. Adv. Mater. 21, 4647–4651.

Murakami, T.N., Grätzel, M., 2008. Counter electrodes for DSC, application of functional materials as catalysts. Inorg. Chim. Acta 361, 572–580.

Nazeeruddin, M.K., De Angelis, F., Fantacci, S., Selloni, A., Viscardi, G., Liska, P., Ito, S., Takeru, B., Gratzel, M., 2005. Combined experimental and DFT-TDDFT computational study of photoelectrochemical cell ruthenium sensitizers. J. Am. Chem. Soc. 127, 16835–16847.

O'Regan, B., Gratzel, M., 1991. A low-cost, high-efficiency solar cell based on dye-sensitized colloidal TiO_2 films. Nature, 353–737.

Olsen, E., Hagen, G., Lindquist, S.E., 2000. Dissolution of platinum in methoxy propionitrile containing LiI/I^{2-}. Sol. Energy Mater. Sol. Cells 63, 267–273.

Papageorgiou, N., 2004. Counter-electrode function in nanocrystalline photoelectrochemical cell configurations. Coord. Chem. Rev. 248, 1421–1446.
Roy-Mayhew, J.D., Bozym, D.J., Punckt, C., Aksay, I.A., 2010. Functionalized graphene as a catalytic counter electrode in dye-sensitized solar cells. ACS Nano 4, 6203–6621.
Siriroj, S., Pimanpang, S., Towannang, M., Maiaugree, W., Phumying, S., Jarernboon, W., Amornkitbamrung, V., 2012. High performance dye-sensitized solar cell based on hydrothermally deposited multiwall carbon nanotube counter electrode. Appl. Phys. Lett. 100, 243303.
Suzuki, K., Yamaguchi, M., Kumagai, M., Yanagida, S., 2003. Application of carbon nanotubes to counter electrodes of dye-sensitized solar cells. Chem. Lett. 32, 28–29.
Takahashi, T., Tsunoda, K., Yajima, H., Ishii, T., 2004. Dispersion and purification of single-wall carbon nanotubes using carboxyl methyl cellulose. Appl. Phys. 43, 3636–3639.
Wang, G., Kuang, S., Zhang, J., Hou, S., Nian, S., 2016. Graphitic carbon nitride/multiwalled carbon nanotubes composites as Pt-free counter electrode for high-efficiency dye-sensitized solar cells. Electrochim. Acta 187, 243–248.
Zhang, D.W., Li, X.D., Li, H.B., Chen, S., Sun, Z., Yin, X.J., Huang, S.M., 2011. Graphene-based counter electrode for dye-sensitized solar cells. Carbon 49, 5382–5388.
Zhu, G., Pan, L., Lu, T., Liu, X., Lv, T., Xu, T., Sun, Z., 2011. Electrophoretic deposition of carbon nanotubes film as counter electrodes of dye-sensitized solar cells. Electrochim. Acta 56, 10288–10291.